WILEY-VCH

Contact-Inhibited ERK Signaling is Determined by Cellular-Resolution Western Blotting

Yizhe Zhang,[a] Isao Naguro,[b] Hiroki Ryuno,[b] and Amy E. Herr*[a]

[a] Dr. Y. Zhang, Prof. A. E. Herr
Department of Bioengineering
University of California, Berkeley
Berkeley, CA, 94720, USA
E-mail: aeh@berkeley.edu

[b] Dr. I. Naguro, H. Ryuno,
Graduate School of Pharmaceutical Sciences
The University of Tokyo
Tokyo, Japan

Supporting information for this article is given via a link at the end of the document.

Abstract: Extracellular signal-regulated kinase (ERK) signaling is essential to regulated cell behaviors, including cell proliferation, differentiation, and apoptosis. The influence of cell-cell contacts on ERK signaling is central to epithelial cells, yet few studies have sought to understand the same in cancer cells, particularly with single-cell resolution. To acquire both phenotypic (cell-contact state) and proteomic profile (ERK phosphorylation) on the same HeLa cells, we prepend high-content, whole-cell imaging prior to endpoint cellular-resolution western blot analyses for hundreds of cancer cells cultured on chip. By indexing the phosphorylation level of ERK in each cell or cell-contact cluster to the imaged cell-contact state, we compare ERK signaling between isolated and in-contact cells. We observe attenuated (~2×) ERK signaling in HeLa cells which are in contact *versus* isolated. Attenuation is sustained when the HeLa cells are challenged with hyperosmotic stress. The contact-dependent differential ERK-phosphorylation corresponds to the differential EGFR distribution on cell surfaces, suggesting the involvement of EGFRs in contact-inhibited ERK signaling. Our findings show the impact of cell-cell contacts on ERK activation with isolated and in-contact cells, hence providing a new tool into control and scrutiny of cell-cell interactions.

Introduction

Cell behaviors are constantly affected by signals from the outside microenvironment such as neighbor cells and extracellular matrix components. As a fundamental cell-cell interaction, physical contact between epithelial cells has been reported to inhibit a wide variety of critical cell activities in culture, including cell growth, proliferation, autophagy, phagocytosis, movement, adhesiveness, and plasticity of stem cells.[1] While knowledge is accumulating towards a comprehensive understanding of contact-inhibited cell processes, research findings have suggested the involvement of pathways of mitogen-activated protein kinases (MAPKs) in the molecular mechanisms of contact inhibition.[2] MAPKs (e.g., ERK1/2, p38α/β/γ/δ, JNK1/2/3) underpin myriad cell activities. Through rapid phosphorylation, MAPKs regulate a wide range of cell processes, including proliferation, differentiation, stress responses, apoptosis, and immune response.[3] Hence, comparative analysis of MAPK activation in isolated *versus* in-contact paired cells should provide additional insight into signal regulation relevant in physiology and pathology.

Studies suggest that contact-inhibition is a local phenomenon rather than a global effect across a layer of cells,[2a] thus creating interest in scrutinizing MAPK activation in different cell-contact states with single-cell resolution. However, the majority of contact-inhibition studies have been performed in bulk. In bulk, behaviors of high-density *versus* low-density cells or interior *versus* peripheral cells in a monolayer have been compared,[1a, 2a, 4] with finer resolution analyses stymied by technological limitations in single-cell culture and analyses. A key challenge is that adherent cells tend to grow in clusters in bulk even at a low seeding density.[5] Depending on the cell-spreading behavior, mixed cell-contact states can appear within each cell-contact group. Hence, it is challenging to obtain information from unambiguously isolated *versus* unambiguously in-contact cells. On the other hand, the lack of effective techniques to detect MAPK activation in mammalian cells with single-cell resolution limits the understanding in this field: conventional assessment of phosphorylation through mass spectrometry or western blotting provides ensemble measurement from a population of cells.[6] Flow cytometry can interrogate millions of single cells for MAPK phosphorylation with high sensitivity. Yet the need for single-cell suspensions leads to the loss of cell-contact information. And the fixative used in the sample preparation can interfere with target epitopes.[7] Newer single-cell resolution assays based on immunocytochemistry or mass spectrometry measurement of

[a] Dr. Y. Zhang, Prof. A. E. Herr
Department of Bioengineering
University of California, Berkeley
Berkeley, CA, 94720, USA
E-mail: aeh@berkeley.edu

[b] Dr. I. Naguro, H. Ryuno
Graduate School of Pharmaceutical Sciences
The University of Tokyo
Tokyo, Japan

Supporting information for this article is available at:
http://dx.doi.org/10.1002/anie.2023xxxxx.

phosphorylation offer limited throughput and require intensive data analysis.[8]

To obtain precision measurement of MAPK in isolated *versus* in-contact cells, we introduce a multi-mode microfluidic assay, called *contact*Blot for brevity: the first mode is whole-cell imaging after on-chip cell culture followed by a second mode which is an endpoint single-cell or contact-cell microwell-based western blot (µWB), wherein the microwell provides short-term cell culture conditions.[9] Here we utilize brightfield whole-cell imaging to visually determine isolated *versus* in-contact status for each cell. We applied the *contact*Blot to HeLa cells to assess ERK phosphorylation under different osmotic conditions (a widely used stress-stimulus for MAPK-signaling studies), and observed differential phosphorylation levels of ERK in isolated- *versus* in-contact cells under each osmotic condition. The in-contact cells exhibit a lower level of ERK activation compared to the isolated-cells. This contact-dependent differential ERK phosphorylation is observed along with differential accumulation of epidermal growth factor receptors (EGFRs) on cell membranes.

Results and Discussion

Determining Phosphorylation Level of Isolated versus In-Contact Cells

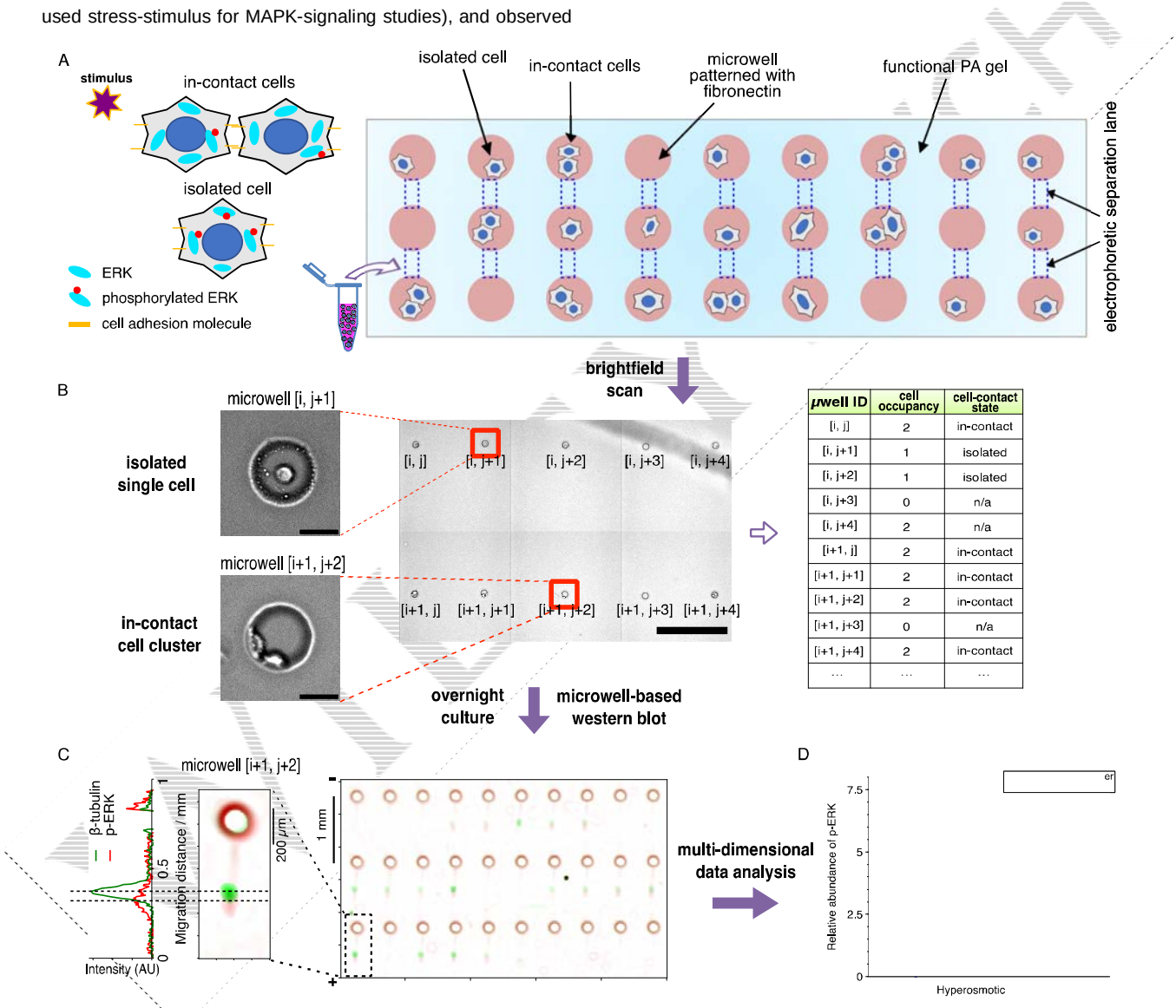

Figure 1. The multi-modal *contact*Blot assay prepends whole-cell brightfield imaging to determine cell contact state (isolated *versus* in-contact) with endpoint single-cell or cell-cluster western blotting (µWB) to measure ERK signaling. A microwell array format underpins concurrent on-chip culture and subsequent analysis of hundreds of isolated and in-contact cells. (A) To study ERK signaling in the context of cell-contact state, epithelial cells are loaded into microwells of a *contact*Blot device for on-chip cell culture. The microwell array is composed of ~2000 microwells stippled in a polyacrylamide (PA) hydrogel layer. The PA gel first acts as the microwell walls and, subsequently, as a µWB protein electrophoresis and blotting gel. Cells are seated in each microwell, the floor of which is functionalized with fibronectin to support spreading of adherent epithelial cells. Microwells are 40 µm deep and 50 µm in diameter to accommodate both individual and clustered HeLa cells. (B) The cell-contact state is determined by brightfield scan (~20 min) of the epithelial cell(s) accommodated in each microwell. After

imaging, cells in the *contact*Blot are cultured on chip for 12 h before endpoint µWB of phosphorylated ERK (p-ERK) under an osmotic stress condition. Brightfield imaging of contact state and fluorescence imaging of the endpoint µWB are indexed to facilitate mapping back to the originating cell, thus reporting same-cell multi-modal profiles. Scale bars: left, 30 µm; middle, 500 µm. (C) Cell ERK signaling state is inferred from the level of p-ERK detected.[9a] (D) Comparative analysis of ERK signaling for isolated *versus* in-contact cells is conducted for each cell-occupied microwell by combining the imaging data with the *in situ* µWB results using the indexing framework.

To correlate heterogeneous cell behaviors with intracellular signaling response, we measure MAPK signaling in single HeLa cells in the context of neighbor cells. In this study, we extend our *in situ* single-cell western blot (*in situ* scWB) previously developed to measure the dynamic phosphorylation of MAPKs in stress-induced single-adherent cells.[9a] While the microwells are used to isolate cells, this study uses the features to facilitate cell-cell contact and the development of any associated intracellular signaling response during a short-term, on-chip cell culture period. The µWB device comprises ~2000 microwells stippled in a thin-layer polyacrylamide gel mounted on a microscope slide (Figure 1A). Cells are gravity settled into the microwells (50 µm in diameter, ~40 µm deep). To support short-term, in-well cell culture, each microwell is functionalized with the extracellular matrix protein fibronectin (Figure S1). In addition to forming the walls of the microwell features, during the endpoint µWB, the polyacrylamide gel toggles between a protein-sieving matrix during protein electrophoresis to being a protein-capture scaffold (blotting membrane) upon brief exposure of the chip to UV light that activates benzophenone methacrylamide in the polymer network. Immobilized protein peaks are probed in-gel using primary and secondary fluorescently labeled antibody probes.[10] To avoid disruptive dissociation of cell clusters, we integrate cell culture and western blotting on the same device for hundreds of individual cells, and hence we interrogate adherent cells in culture with single-cell resolution.

To perform comparative analysis of MAPK signaling on single isolated *versus* in-contact cells, the *contact*Blot assay comprises four steps, with details provided in the Supporting Information: (1) Gravity settle a cell suspension on the face of the open microfluidic device using an optimized cell-suspension density, so that the single-cell and two-cell microwell occupancies are dominant and sufficient for statistical analysis. (2) During a brief incubation period (~1.5 h), adherent cells attach to the microwell walls through weak bonds with the fibronectin-decorated microwells. The cell-contact state of cells in each microwell is measured via brightfield microscopy inspection of the entire device (Figure 1B). This slide-scan step can be repeated, acquiring state across multiple time points. The brightfield scanning period (~20 min) imparts negligible perturbation to the system under study (Figure S2). (3) Application of osmotic stress for 60-min by buffer exchange, using an isosmotic (300 mOsm) or a hyperosmotic (500 mOsm) condition. (4) Completion of the µWB step, with indexing of the endpoint µWB result for each cell-occupied microwell to the image-based cell-contact state (Figure 1C). In endpoint µWB quantitation, β-tubulin signal intensity was used for normalization to rule out the cell-size effect from protein-abundance analysis. In multi-cell occupancy, β-tubulin normalization also generates a cell-number-average result. Depending on cell-occupancy, a blot data point from µWB reports proteomic information from a single cell (single-cell occupancy) or an average of a cell cluster (multi-cell occupancy). Same-cell indexing allows data analyses to differentiate between signaling response in the isolated cells *versus* that in the in-contact cells (Figure 1D). As such, we assess cells' MAPK signaling and contact states simultaneously from a *contact*Blot experiment.

HeLa Cells Exhibit ERK Activation in Response to Osmotic Stress Regardless of Cell-Contact States

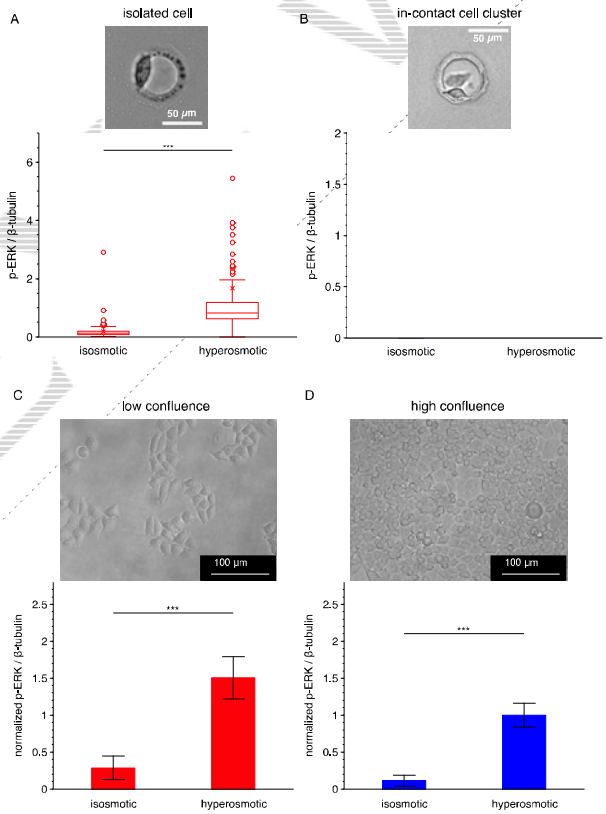

Figure 2. *contact*Blot reports ERK activation levels of HeLa cells in response to hyperosmotic stress that are similar for both isolated and in-contact cells, in agreement with bulk measurements. (A-B) Osmotic response of single isolated (A) and in-contact (B) HeLa cells via ERK signaling. Top, representative bright-field micrographs (10× objective) of HeLa cells cultured in the microwell. Bottom, box plots showing the β-tubulin-normalized p-ERK levels from µWB measurements. Over 100 µWB assays are analyzed for each µWB experiment. Upon a 60-min application of the hyperosmotic stress of 500 mOsm, a significant increase of p-ERK is detected regardless of the cell-contact states, with the increase fold of 6.4× and 6.1× in the median p-ERK level for isolated and in-contact cells, respectively. Statistical analysis is performed with the Mann-Whitney *U* test. ***$P < 0.001$. Scale bars: 50 µm. (C-D) Osmotic

response of low-confluence (C) and high-confluence (D) HeLa cells in ERK signaling. Top, representative brightfield micrographs (20× objective) of HeLa cells cultured in the bulk experiments. The seeding cell numbers are 2.5 x 10^4 and 20 x 10^4 for low- and high-confluence experiments, respectively. Bottom, bar plots showing the β-tubulin-normalized p-ERK levels from bulk measurements. Data are presented as means ± SDs (n > 3). Upon a 60-min application of the hyperosmotic stress condition, a significant increase of p-ERK is detected regardless of the cell-confluence level. Statistical analysis is performed with the one-tailed Student's t-test. ***P < 0.001. Scale bars: 100 µm.

To validate the *contact*Blot assay, we examine ERK activation in response to hyperosmotic stress for isolated and in-contact cells. In HeLa cells, we have previously observed marked activation of the typical MAPKs (ERK, p38) induced by the hyperosmotic stress in single-cell and bulk experiments.[9a] Using the *contact*Blot assay, we measure both isolated cells and in-contact cells and – for both phenotypes – observe a significant increase in the level of the phosphorylated-ERK (p-ERK; normalized to β-tubulin) upon application of the hyperosmotic stress (Figure 2A and 2B; Mann-Whitney U test, n > 100 blots, $P_{isolated}$ = 2.139 x 10^{-49}, $P_{in\text{-}contact}$ = 1.065 x 10^{-11}). In the isolated-cell group, the hyperosmotic-stress-induced increase of the median p-ERK is 6.4×, in agreement with current understanding.[9a, 11] For the in-contact cell group under hyperosmotic stress, we observe a comparable increase in median p-ERK (6.1×). These observations suggest hyperosmotic stress induces similar ERK-activation regardless of the cell-contact state.

To validate the µWB assessment, we perform bulk western blotting of cell groups, where we tune the cell confluency to represent the cell-contact state (Figure 2C and 2D). In the population-averaged slab-gel western-blot measurements, we observe a significant increase in the p-ERK level (normalized to β-tubulin) induced by the hyperosmotic stress condition in both low-confluence (2.5 x 10^4 cells) and high-confluence (20 x 10^4 cells) groups (one-tailed Student's t-test, n > 3, $P_{low\text{-}confluence}$ = 4.503 x 10^{-4}, $P_{high\text{-}confluence}$ = 2.557 x 10^{-6}). In sum, comparable ERK-activation stress-response levels are observed in the population-wide groups, regardless of cell-contact state.

The validation study suggests that *contact*Blot reports cellular-resolution ERK phosphorylation under hyperosmotic stress, as is consistent with previous reports. Furthermore, *contact*Blot shows comparable ERK-activation levels between the isolated *versus* in-contact cells in response to hyperosmotic stress.

HeLa Cells Exhibit Attenuated ERK Signaling in the In-Contact Cell Group

Having validated the *contact*Blot assay on hyperosmotic-stress-induced ERK activation, we next seek to understand the role of cell-cell contact on signal transduction. Cell-cell contacts have been largely reported to inhibit the activity of epithelial cells in bulk.[1] Because of the clustering tendency of adherent cells, analyzing cells in bulk provides limited insight. Using precision microfluidic analytical tools, we aim to examine the ERK signaling with unambiguously isolated and in-contact cells to gain more precise understanding of the role of cell-contact state.

We first examine the p-ERK levels under the isosmotic condition for both isolated cells and in-contact cells (Figure 3A). We make two key observations: (1) the median p-ERK level in the in-contact cell group is significantly lower than in the isolated-cell group (Mann-Whitney U test; n > 100 cells, P = 7.695 x 10^{-11} for replicate 1, n > 50 cells, P = 1.008 x 10^{-9} for replicate 2), and (2) the median p-ERK level in the in-contact cell group is ~50% of that same value in the isolated-cell group (0.56× for replicate 1, 0.42× for replicate 2).

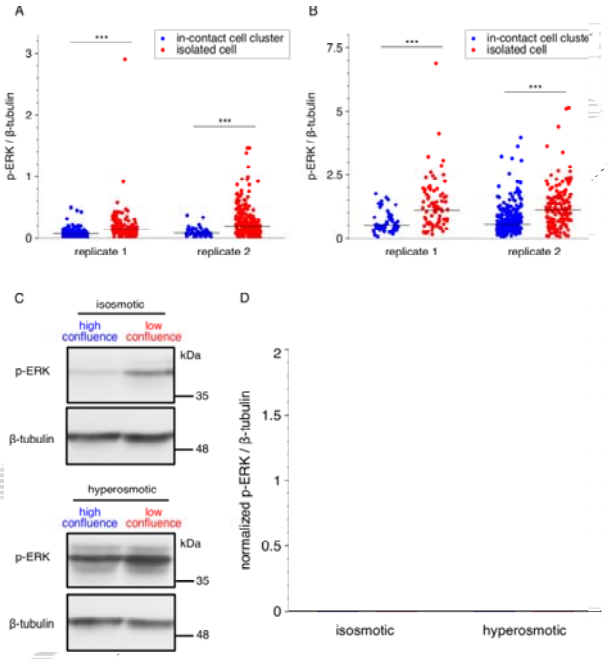

Figure 3. *contact*Blot reports differential ERK activation between the isolated and in-contact HeLa cells. (A-B) HeLa cells exhibit a significantly attenuated ERK activation level in in-contact *versus* isolated single cells. The contact-attenuation in ERK activation is observed under both the isosmotic (A) and hyperosmotic (B) conditions. Solid lines across the data sets denote the median level. Statistical analysis is performed with the Mann-Whitney U test. ***P < 0.001. Over 100 µWBs are analyzed for each µWB experiment. (C) Bulk western blotting of a population of HeLa cells confirms the attenuated activation of ERK in high-confluence cells (full-size gels in Supporting Information). The seeding cell numbers are 2.5 x 10^4 and 20 x 10^4 for low- and high-confluence experiments, respectively. β-tubulin is used as a loading control. (D) Quantitative analysis of ERK differential activation in low- and high-confluence cells from the population-level western blotting experiments. The difference in the ERK activation levels between the cells in high- and low-confluence is not significant under the isosmotic condition and marginally significant under the hyperosmotic condition, yet less pronounced than observed with *contact*Blot. Data are presented as means ± SDs (n > 3). Statistical analysis is the one-tailed Student's t-test. *P < 0.05; n.s., P > 0.05.

Next, to understand the impact of cell-cell contact on the acute stress responses, we investigate ERK phosphorylation levels at the end of the 60-min hyperosmotic shock. By comparing the p-ERK levels between the isolated-cells and in-contact cells,

analysis can shed light on the differential phosphorylation levels of ERK as related to cell-contact state, after the hyperosmotic treatment (Figure 3B). We observe that the median p-ERK level in the in-contact cell group is significantly lower than the value measured in the isolated-cell group (Mann-Whitney *U* test; n > 50 cells, $P = 1.496 \times 10^{-6}$ for replicate 1, n > 150 cells, $P = 4.055 \times 10^{-16}$ for replicate 2). We further observe that the differences in the median p-ERK level between the isolated and the in-contact cell groups are 0.45× and 0.50× for replicate 1 and 2, respectively.

In contrast, in bulk assays (where no physical confinement is imposed) HeLa cells tend to grow in clusters even at a low seeding density (Figure 2C), thus presenting challenging ambiguity in analyses of isolated (no cell-cell contact) cells. Consequently, assessing the difference in p-ERK levels between isolated and in-contact cells is challenging using bulk cell culture approaches. For comparison, we analyze the bulk data in Figure 2, and observe a lower p-ERK level in the highly confluent cells (assuming mostly in-contact cells) compared to the low-confluence cells (Figure 3C and 3D), but the difference is less pronounced as compared to the degree of difference observed in *contact*Blot experiments (one-tailed Student's *t*-test, n > 3 replicates; $P = 0.015$ for the hyperosmotic condition, $P = 0.056$ for the isosmotic condition). We attribute the subtle difference observed in the slab-gel western blot to i) the inclusion of a population of in-contact cells in even the low-confluence group and ii) insufficient detection sensitivity for lower abundance protein targets under the isosmotic conditions in the low-confluence group. Two confounding factors that can be readily addressed with enhanced precision in *contact*Blot in cell handling and analysis.

Taken together, we observe an attenuated level of p-ERK in the in-contact cell group under both hyperosmotic and isosmotic conditions. The differential levels of p-ERK between the isolated and in-contact cells are distinguishable using the precision *contact*Blot because: i) cell confinement in microwells enforces an isolated cell state as compared to standard plate cell culture, ii) *in-situ* analyses during cell culture reduce perturbations from cell-sample preparation and handling, and iii) relatively weak signals from the endpoint µWB of single, isolated cells under the isosmotic condition are detectable using the photomultiplier tube-based fluorescence detection.

In-Contact HeLa Cells Exhibit Reduced Levels of EGFRs on the Membrane Compared to Isolated HeLa Cells

To understand the processes involved in attenuation of p-ERK in the in-contact cells, we seek to scrutinize the spatial organization of the EGFRs on the surface of these cells. EGFRs are understood to be core to sensing and transducing signals from a variety of environmental stimuli in mammalian cells.[12] Under the hyperosmotic stress, EGFRs on the cell membrane are observed to form clusters and to be internalized, concomitant with the phosphorylation of MAPKs.[13] Therefore, we hypothesize that the attenuated p-ERK level in the in-contact cells is associated with a distinct EGFR distribution on the cell surface.

To scrutinize this hypothesis, we used immunocytochemistry (Supporting Information) and observed that the average fluorescence of EGFRs is significantly reduced under the hyperosmotic condition for both isolated and in-contact cells (Figure 4A, 4C and 4E; Mann-Whitney *U* test; n > 30 cells, $P = 7.920 \times 10^{-4}$ for the isolated cells, n > 20 cells, $P = 3.657 \times 10^{-4}$ for the in-contact cells). The decrease in the average fluorescence of EGFRs upon application of the hyperosmotic stress is consistent with previously observed internalization and degradation of EGFRs induced by this external stimulus.[13d-f]

Under the normal osmotic condition, we note that intracellular EGFRs remain at a noticeably high level. Compared to the membrane-concentrated distribution of EGFRs in the serum-starved cells,[14] the observed elevated abundance of EGFRs in the nucleus and cytoplasm in our study is attributed to the stimulating growth factors in the fetal bovine serum (FBS, 10% v/v) of the complete cell-culture media.[15] Similar subcellular EGFR distributions were observed by others in MCF-7 cells cultured in the FBS-supplemented cell culture media.[16]

The whole-cell average fluorescence of EGFRs reports: 1) differential EGFR levels under the normal and hyperosmotic stress conditions and 2) no significant EGFR-level difference between the isolated and in-contact cells under the same osmotic condition (Figure 4E; Mann-Whitney *U* test; n > 20 cells, $P = 0.6441$ for the isosmotic condition; n > 40 cells, $P = 0.3980$ for the hyperosmotic condition).

Given the high abundance of EGFRs in the nucleus and cytoplasm observed here, we surmise that whole-cell average fluorescence may obscure the distribution of EGFRs localized to the cell surface membrane. To measure membrane EGFR levels, we thus specifically use EGFR signals from the cell membrane and plot the membrane fluorescence intensity as a function of the angle (Figure 4B and 4D; Figure S3 and S4). In the resultant angular distribution curves of membrane EGFRs, we observe characteristic signal spikes on individual cells or cell clusters (Figure 4B and 4D, asterisks; Figure S5), corresponding to observed signal clusters along the edge of the cell (Figure 4A and 4C, arrows). The spike number and amplitudes are suggestive of the known cell-contact state. To quantify the spikes in the angular distribution curves of the membrane EGFRs, we calculate the spike number (N_{spike}), mean spike intensity (i_{spike}) and total spike intensity (I_{spike}) for each cell or cell cluster (Table S1-S5 and Figure S6-S9). To discern the spike features from the baseline fluorescence, we subtract the baseline fluorescence intensity ($I_{baseline}$) and consider the relative intensity of the signal spikes (Table S2-S5 and Figure S10).

Under the normal osmotic condition, I_{spike} is significantly different between the isolated cells and in-contact cells (Mann-Whitney *U* test; n > 40 cells, $P = 0.0430$). The median I_{spike} in the isolated-cell group is 2.46× of the median I_{spike} of the in-contact cell group. Further, under the hyperosmotic condition, I_{spike} in the in-contact cells remains lower than in isolated cells (0.84× in median level), but the difference is not as significant (Mann-Whitney *U* test; n > 50 cells, $P = 0.4233$) (Figure 4F). We attribute the decrease of the contact-dependent difference in the membrane EGFR level under the hyperosmotic stress to the stress-induced rearrangement of EGFRs.[13c-f] Further scrutiny reveals that the

significant difference in I_{spike} under the normal osmotic condition between the isolated and in-contact cells is attributed to the differential N_{spike} between the isolated and in-contact cells (Figure 4G; Mann-Whitney *U* test; $n > 40$ cells, $P = 0.0007$ for the normal osmotic condition). We also find that there is no significant difference in i_{spike} between the isolated and in-contact cells under the normal or hyperosmotic condition (Figure 4H; Mann-Whitney *U* test; $n > 40$ cells, $P = 0.9623$ for the normal osmotic condition; $n > 50$ cells, $P = 0.4040$ for the hyperosmotic condition).

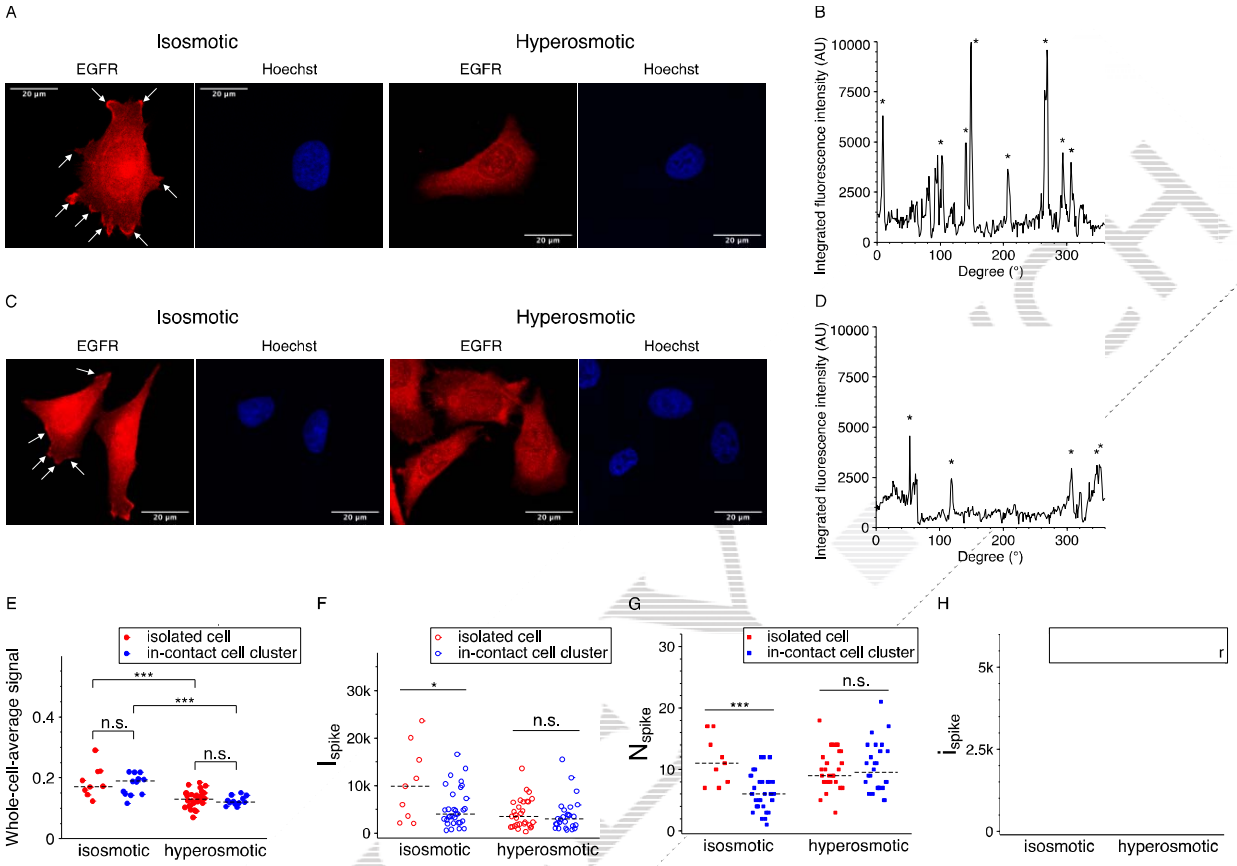

Figure 4. Differential distribution of cell surface membrane EGFRs between isolated and in-contact HeLa cells. (A) Representative fluorescence micrographs of EGFR distribution in the immunoprobed isolated HeLa cells under the normal and hyperosmotic-stress conditions. Red, fluorescently labeled anti-EGFR antibody probes. Blue, the Hoechst 33342 nuclear stain. The arrows denote the regions where EGFRs accumulate. The isosmotic and hyperosmotic conditions are 60 min exposure to 300 and 500 mOsm solutions, respectively. Scale bars: 20 µm. (B) The angular EGFR fluorescence intensity distribution on the cell membrane for an isolated cell under the isosmotic condition in (A). The asterisks denote signal spikes which may represent accumulated EGFR clusters as indicated in the fluorescence micrograph. (C) Representative fluorescence micrographs of EGFR distribution from immunoprobed in-contact HeLa cells under normal and hyperosmotic-stress conditions. (D) The angular EGFR fluorescence intensity distribution on the cell membrane for the in-contact cell under the isosmotic condition in (C). (E-H) Scatter plots of EGFR abundance (E) and EGFR membrane distribution (F-H) for individual cells or cell clusters. For brevity, the total spike intensity, spike number, and mean spike intensity for each cell or cell cluster are denoted by I_{spike}, N_{spike}, and i_{spike}. Dashed lines denote the median level. To extract EGFR cell surface membrane signals for different cell-contact states, baseline-subtracted signal spikes in the angular intensity profile were used (Supporting Information). Statistical analysis is performed with Mann-Whitney *U* test. ***$P < 0.001$; **$P < 0.01$; *$P < 0.05$; n.s., not significant at the 5% significance level. >20 µWB results are analyzed for each *contact*Blot experiment.

The observation of differential ERK signaling between the isolated and in-contact cells under isosmotic conditions is in alignment with the growth-promoting function of ERKs. As a ubiquitous MAPK protein responding to growth factors (e.g., EGF), activated ERKs promote cell-cycle entry by regulating the expression of Cyclin D1.[2a, 17] Hence, the inhibited growth and division in in-contact cells would involve a shift of the ERK activation state from the state in isolated cells. In fact, lower p-ERK levels in high-density cells are common in epithelial cell lines,[1b, 2b, 18] consistent with our observations. Interestingly, under hyperosmotic stress we observe differential ERK signaling between isolated- and in-contact cells, and the difference in the median level of p-ERK is comparable to the difference at the isosmotic level. Combining with the comparable hyperosmotic-stress-induced ERK activation levels between the isolated- and in-contact cells, our study suggests that 1) under the

hyperosmotic condition, the observed differential p-ERK levels between the isolated- and in-contact cells arise from the attenuated p-ERK level in the in-contact cells occurring in culture and 2) an acute osmotic shock generates comparable fold changes in ERK response in isolated- and in-contact cells.

Contact-inhibited cell behavior has been extensively studied in normal epithelial cells (e.g., fibroblasts, MCF-10A cells, Madin-Darby canine kidney (MDCK) cells).[1b, 2a, 18] Cancer cells are typically considered to lack contact-inhibition even in high-confluence populations.[19] Reports have suggested that the loss of contact-inhibition features may be a hallmark of cancer.[1b, 20] However, inhibited growth of HeLa cells was noticed in an early microscopic study of cellular contact behaviors, where piling or strong overlapping of cells was not detected.[21] In addition to HeLa cells, the typical breast cancer cell line MCF-7 has been reported to exhibit contact-inhibited proliferation.[4] By identifying the existence of contact-attenuated p-ERK in HeLa cells, our findings, along with other contact-inhibition studies on cancer cells, suggest that contact-inhibited activity exists in certain cancer cell lines, and loss of contact-inhibition may not be a generic hallmark for cancer cells, at least not in some *in vitro* cultured cancer cell lines. Understanding the regulation of cancer cell activities in the context of cell-cell contacts would facilitate molecular studies of tumor progression.

Here, we observed differential EGFR cell-surface expression between the isolated- and in-contact cells. The differential EGFR levels are in line with the differential p-ERK levels measured in the isolated *versus* in-contact cells. Intriguingly, at the isosmotic level, the EGFR cell-surface expression is comparable to the difference in p-ERK level (~2×) between the two cell-contact groups. The comparable levels of EGFR and p-ERK expression merits further study, as the correlation may suggest the involvement of the membrane receptor EGFR in the contact-induced attenuation of p-ERK. In fact, previous studies have reported the rearrangement of membrane proteins (including EGFRs) upon cell-cell contact.[22] The rearrangement of membrane EGFRs could be a combined effect of lateral transport, clustering, and internalization in response to the changing context in culture.[13e, f] These cellular-resolution, multi-modal results suggest candidate regulator proteins may exist, beyond the extensively investigated regulators such as E-cadherin.[4, 14a] While speculative at this point, comprehensive mechanistic understanding of contact-inhibited cell activities is needed. Microfluidic analytical tools provide important avenues towards that goal.

While this study focuses on ERK activation given relevance in regulating cell proliferation, the interplay of MAPKs in coordinating cell responses to environmental stimuli suggests potential differential activation for other kinases in the MAPK family, such as p38 and JNK. Attenuated levels of p-p38 and p-JNK were observed in fibroblasts in bulk experiments.[23] Our bulk data support this hypothesis with HeLa cells (Figure S11). More broadly, enzymes that participate in the regulation of MAPKs, such as tumor necrosis factor receptor 1 (TNFR1), MAP kinase kinase (MKK), and MAP kinase phosphatase (MKP), may also be candidates expressing differential activation levels between isolated and in-contact cellular conditions.

While this study observes an attenuated level of activated ERKs in the in-contact HeLa cells, we cannot rule out possible effects from other differential environmental cues imposed on the cells of different contact states. For example, bioactive molecules that are secreted or consumed by a cell can be present at differential local concentrations in a cell-contact-relevant manner. In fact, the change of radical levels related to cellular metabolic activities can alter the local redox environment. The alteration in local redox environment correlates with contact-inhibited proliferation across cell lines.[24] The observed attenuation of p-ERK in the in-contact cells could very likely be a combined effect involving both the physical cue of cell-cell contact and the chemical cues emanating from proximal cells. Future studies could include finer classification of cell-cell interactions (i.e., consideration of the cell-cell distance in the isolated-cell group, profiling of secreted factors) to create a holistic understanding of the milieu created during cell-cell contact.

Conclusion

We introduce, validate, and apply an imaging-facilitated *in situ* cellular-resolution western blot (*contact*Blot) assay that reports cell-contact information and protein signaling activity for an array of hundreds of individual cells. This multi-modal analysis tool provides comparative targeted proteomic analyses of cancer cells, both in isolation and in contact with neighboring cells. Such profiling may clarify differential protein levels in early and late phases of tumor development, hence facilitating analysis of new cancer-drug targets related to cell-cell contact. Differential stress responses of isolated and in-contact cells may delineate therapeutic susceptibility of diseased cells at different stages in disease progression, thereby informing treatment decisions. Furthermore, by including various fluorescent probes in imaging, the *contact*Blot assay indexes the μWB-derived targeted proteomic signatures of individual cells to a broader range of physical and biochemical conditions of the same cells, including intracellular temperature,[25] membrane potentials,[26] O_2 levels,[27] pH levels,[28] and cell-cycle phases.[29]

Supporting Information

Experimental details, including reagents, device fabrication, assay protocols, and statistics are provided in the Supporting Information. The authors have cited additional references within the Supporting Information.[30-32]

Acknowledgements

This work was supported by the US National Institutes of Health (R01CA203018 and R33CA225296 to A. E. H.), the Chan Zuckerberg Biohub (to A. E. H.), and JSPS KAKENHI (Grant Number JP15KK0297 and JP18H02569 to I. N.). We thank the QB3 Biomolecular Nanotechnology Center in Stanley Hall and the CRL Molecular Imaging Center (supported by the Helen

Wills Neuroscience Institute) at the University of California, Berkeley. We appreciate helpful discussions with Herr Lab members throughout this project. Henrietta Lacks, and the HeLa cell line that was established from her tumor cells without her knowledge or consent in 1951, have made significant contributions to scientific progress and advances in human health. We are grateful to Henrietta Lacks, now deceased, and to her surviving family members for their contributions to biomedical research. The content is solely the responsibility of the authors and does not represent the official views of the National Institutes of Health.

Keywords: Electrophoresis • Gels • Materials science • Microarrays • Phosphorylation

[1] a) N.-G. Kim, E. Koh, X. Chen, B. M. Gumbiner, *Proc. Natl. Acad. Sci. U.S.A.* **2011**, *108*, 11930; b) J.-H. Kim, K. Kushiro, N. A. Graham, A. R. Asthagiri, *Proc. Natl. Acad. Sci. U.S.A.* **2009**, *106*, 11149; c) L. Schutz, P. T. Mora, *J. Cell. Physiol.* **1968**, *71*, 1; d) M. Pavel, M. Renna, S. J. Park, F. M. Menzies, T. Ricketts, J. Füllgrabe, A. Ashkenazi, R. A. Frake, A. C. Lombarte, C. F. Bento, K. Franze, D. C. Rubinsztein, *Nat. Commun.* **2018**, *9*, 2961; e) J. M. Vasiliev, I. M. Gelfand, L. V. Domnina, O. S. Zacharova, A. V. Ljubimov, *Proc. Natl. Acad. Sci. U.S.A.* **1975**, *72*, 719; f) K. M. Yamada, S. S. Yamada, I. Pastan, *Proc. Natl. Acad. Sci. U.S.A.* **1976**, *73*, 1217; g) J. R. Davis, A. Luchici, F. Mosis, J. Thackery, J. A. Salazar, Y. Mao, G. A. Dunn, T. Betz, M. Miodownik, B. M. Stramer, *Cell* **2015**, *161*, 361; h) T. Wang, Z. Xu, W. Jiang, A. Ma, *Int. J. Cardiol.* **2006**, *109*, 74.

[2] a) A. Puliafito, L. Hufnagel, P. Neveu, S. Streichan, A. Sigal, D. K. Fygenson, B. I. Shraiman, *Proc. Natl. Acad. Sci. U.S.A.* **2012**, *109*, 739; b) S. Li, E. R. Gerrard, Jr., D. F. Balkovetz, *Am. J. Physiol. Cell Physiol.* **2004**, *287*, C432; c) Y. Matsubayashi, M. Ebisuya, S. Honjoh, E. Nishida, *Curr. Biol.* **2004**, *14*, 731.

[3] a) G. L. Johnson, R. Lapadat, *Science* **2002**, *298*, 1911; b) G. Pearson, F. Robinson, T. G. Gibson, B.-E Xu, M. Karandikar, K. Berman, M. H. Cobb, *Endocr. Rev.* **2001**, *22(2)*, 153; c) M. Cargnello, P. P. Roux, *Microbiol. Mol. Biol. Rev.* **2011**, *75*, 50; d) W. Zhang, H. T. Liu, *Cell Res.* **2002**, *12(1)*, 9; e) J. Hirosumi, G. Tuncman, L. Chang, C. Z. Görgün, K. T. Uysal, K. Maeda, M. Karin, G. S. Hotamisligil, *Nature* **2002**, *420*, 333; f) C. Dong, R. J. Davis, R. A. Flavell, *Annu. Rev. Immunol.* **2013**, *13*, 679; g) J. Simon, C. Arthur, S. C. Ley, *Nat. Rev. Immunol.* **2013**, *13*, 679.

[4] C. A. Kumamoto, *Proc. Natl. Acad. Sci. U.S.A.* **2005**, *102*, 5576.

[5] a) C. D. Helgason in *Basic Cell Culture Protocols* (Eds.: C. D. Helgason, C. L. Miller), Humana Press, Totowa, New Jersey, **2005**, pp. 1–12; b) F. Ortega, M. R. Costa, T. Simon-Ebert, T. Schroeder, M. Götz, B. Berninger, *Nat. Protoc.* **2011**, *6*, 1847.

[6] a) M. J. Rust, J. S. Markson, W. S. Lane, D. S. Fisher, E. K. O'Shea, *Science* **2007**, *318*, 809; b) K. Aoki, M. Yamada, K. Kunida, S. Yasuda, M. Matsuda, *Proc. Natl. Acad. Sci. U.S.A.* **2011**, *108*, 12675.

[7] J. Brummelman, C. Haftman, N. G. Núñez, G. Alvisi, E. M. C. Mazza, B. Becher, E. Lugli, *Nat. Protoc.* **2019**, *14*, 1946.

[8] a) V. Marx, *Nat. Methods* **2019**, *16*, 809; b) A. H. C. Ng, M. D. Chamberlain, H. Situ, V. Lee, A. R. Wheeler, *Nat. Commun.* **2015**, *6*, 7513.

[9] a) Y. Zhang, I. Naguro, A. E. Herr, *Angew. Chem. Int. Ed.* **2019**, *58*, 13929; b) C.-C. Kang, J.-M. G. Lin, Z. Xu, S. Kumar, A. E. Herr, *Anal. Chem.* **2014**, *86(20)*, 10429.

[10] C.-C. Kang, K. A. Yamauchi, J. Vlassakis, E. Sinkala, T. A. Duncombe, A. E. Herr, *Nat. Protoc.* **2016**, *11*, 1508.

[11] a) T. Maruyama, H. Kadowaki, N. Okamoto, A. Nagai, I. Naguro, A. Matsuzawa, H. Shibuya, K. Tanaka, S. Murata, K. Takeda, H. Nishitoh, H. Ichijo, *EMBO J.* **2010**, *29*, 2501; b) M.-B. Nielsen, S. T. Christensen, E. K. Hoffmann, *Am. J. Physiol. Cell Physiol.* **2008**, *294*, C1046.

[12] a) K. Peng, Q. Dai, J. Wei, G. Shao, A. Sun, W. Yang, Q. Lin, *Cancer Cell Int.* **2016**, *16*, 25; b) T. Uyemura, H. Takagi, T. Yanagida, Y. Sako, *Biophys. J.* **2005**, *88*, 3720; c) I. Pinilla-Macua, S. C. Watkins, A. Sorkin, *Proc. Natl. Acad. Sci. U.S.A.* **2016**, *113*, 2122.

[13] a) C. Rosette, M. Karin, *Science* **1996**, *274*, 1194; b) E. d. Nadal, P. M. Alepuz, F. Posas, *EMBO Rep.* **2002**, *3*, 735; c) O. M. Fischer, S. Hart, A. Gschwind, N. Prenzel, A. Ullrich, *Mol. Cell. Biol.* **2004**, *24*, 5172; d) S. Zhang, B. M. Reinhard, *J. Phys. Chem. B* **2019**, *123*, 5494; e) R. Heukers, J. F. Vermeulen, F. Fereidouni, A. N. Bader, J. Voortman, R. C. Roovers, H. C. Gerritsen, P. M. P. v. B. e. Henegouwen, *J. Cell Sci.* **2013**, *126*, 4900; f) N. Bag, S. Huang, T. Wohland, *Biophys. J.* **2015**, *109*, 1925.

[14] a) P. Nagy, J. Claus, T. M. Jovin, D. J. Arndt-Jovin, *Proc. Natl. Acad. Sci. U.S.A.* **2010**, *107*, 16524; b) A. H. Kesarwala, M. M. Samrakandi, D. Piwnica-Worms, *Cancer Res.* **2009**, *69*, 976; c) D. Li, F. Chen, J. Ding, N. Lin, Z. Li, X. Wang, *Oncol. Rep.* **2017**, *38*, 3387.

[15] S.-Y. Lin, K. Makino, W. Xia, A. Matin, Y. Wen, K. Y. Kwong, L. Bourguignon, M.-C. Hung, *Nat. Cell Biol.* **2001**, *3*, 802.

[16] A. Angelin, S. Weigel, R. Garrecht, R. Meyer, J. Bauer, R. K. Kumar, M. Hirtz, C. M. Niemeyer, *Angew. Chem. Int. Ed.* **2015**, *54*, 15813.

[17] a) A. K. Fournier, L. E. Campbell, P. Castagnino, W. F. Liu, B. M. Chung, V. M. Weaver, C. S. Chen, R. K. Assoian, *J. Cell Sci.* **2008**, *121*, 226; b) S. L. Pelech, D. L. Charest, *Prog. Cell Cycle Res.* **1995**, *1*, 33; c) J. D. Weber, D. M. Raben, P. J. Phillips, J. J. Baldassare, *Biochem. J.* **1997**, *326*, 61; d) R. Steinmetz, H. A. Wagoner, P. Zeng, J. R. Hammond, T. S. Hannon, J. L. Meyers, O. H. Pescovitz, *Mol. Endocrinol.* **2004**, *18*, 2570.

[18] J. Wayne, J. Sielski, A. Rizvi, K. Georges, D. Hutter, *Mol. Cell. Biochem.* **2006**, *286*, 181.

[19] M. Abercrom, E. J. Ambrose, *Cancer Res.* **1962**, *22*, 525.

[20] D. Hanahan, R. A. Weinberg, *Cell* **2000**, *100*, 57.

[21] a) K. Knyrim, N. Pawelet, *Virchows Arch. B Cell Pathol.* **1978**, *28*, 243; b) M. Abercrombie, *Nature* **1979**, *281*, 259.

[22] a) I. Chow, M.-M. Poo, *J. Cell Biol.* **1982**, *95*, 510; b) C. T. Mierke in *Physics of Cancer* (Ed.: C. T. Mierke), IOP Publishing, Bristol, **2015**, pp. 7.1–7.32.

[23] M. Slisz, E. Rothenberger, D. Hutter, *Mol. Cell. Biochem.* **2008**, *308*, 65.

[24] a) D. E. Hutter, B. G. Till, J. J. Greene, *Exp. Cell Res.* **1997**, *232*, 435; b) F. Q. Schafer, G. R. Buettner, *Free Radic. Biol. Med.* **2001**, *30*, 1191.

[25] a) K. Okabe, N. Inada, C. Gota, Y. Harada, T. Funatsu, S. Uchiyama, *Nat. Commun.* **2012**, *3*, 705; b) K. Okabe, R. Sakaguchi, B. Shi, S. Kiyonaka, *Pflugers Arch. – Eur. J. Physiol.* **2018**, *470*, 717.

[26] S. W. Perry, J. P. Norman, J. Barbieri, E. B. Brown, H. A. Gelbard, *Biotechniques* **2011**, *50*, 98.

[27] R. I. Dmitriev, D. B. Papkovsky, *Cell. Mol. Life Sci.* **2012**, *69*, 2025.

[28] J.-W. Chen, C.-M. Chen, C.-C. Chang, *Org. Biomol. Chem.* **2017**, *15*, 7936.

[29] S. Yano, R. M. Hoffman, *Cells* **2018**, *7*, 168.

[30] Novus Biologicals, "Protocol of Immunocytochemistry (ICC)", can be found under https://www.novusbio.com/support/support-by-application/immunocytochemistry/protocol.html (accessed: **2023**).

[31] A. E. Carpenter, T. R. Jones, M. R. Lamprecht, C. Clarke, I. H. Kang, O. Friman, D. A. Guertin, J. H. Chang, R. A. Lindquist, J. Moffat, P. Golland, D. M. Sabatini, *Genome Biol.* **2006**, *7*, R100.

[32] G. L. Ryan, N. Watanabe, D. Vavylonis, *Cell Struct. Funct.* **2013**, *38*, 1.

WILEY-VCH

Table of Contents

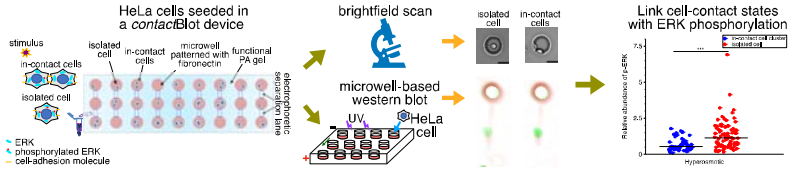

Linking a single cell's biophysical cues with intracellular signaling response: The *contact*Blot multi-modal tool reports same-cell biophysical state (isolated *versus* in-contact cell state) and biochemical response (ERK-phosphorylation level) by integrating brightfield whole-cell imaging with cellular-resolution western blotting.